Marine Pollution Bulletin 135 (2018) 386–396

Contents lists available at ScienceDirect

Marine Pollution Bulletin

journal homepage: www.elsevier.com/locate/marpolbul

Using a genetic algorithm to improve oil spill prediction

Weijun Guo[a], Meirong Jiang[b], Xueyan Li[c], Bing Ren[d,*]

[a] College of Environmental Sciences and Engineering, Dalian Maritime University, Dalian 116026, China
[b] CNOOC Research Institute, Beijing 100028, China
[c] Coast Institute, Ludong University, Yantai 264025, China
[d] The State Key Laboratory of Coastal and Offshore Engineering, Dalian University of Technology, Dalian 116024, China

ARTICLE INFO

Keywords:
Oil spill
Model evaluation
Parameter optimisation
Genetic algorithm

ABSTRACT

The performance of oil spill models is strongly influenced by multiple parameters. In this study, we explored the ability of a genetic algorithm (GA) to determine optimal parameters without the need for time-consuming manual attempts. An evaluation function integrating the percentage of coincidence between the predicted polluted area and the observed spill area was proposed for measuring the performance of a Lagrangian oil particle model. To maximise the objective function, the oil spill was run numerous times with continuously optimised parameters. After many generations, the GA effectively reduced discrepancies between model results and observations of a real oil spill. Subsequent validation indicated that the oil spill model predicted oil slick patterns with reasonable accuracy when equipped with optimal parameters. Furthermore, multiple objective optimisation for observations at different times contributed to better model performance.

1. Introduction

Oil spills are a major environmental concern and regarded as one of worst types of marine pollution, some of which may have disastrous consequences for open oceans and coastal seas. Considerable research has been conducted on the transport of spilled oil using field and laboratory investigations. Numerical oil spill models, which predict the transport and behaviour of oil spills, are an essential instrument for risk assessment and clean-up during an actual accident. However, it is still not possible to predict the actual trajectories of oil spills with any degree of certainty. Over the last three decades, numerous detailed oil spill models have been presented with the goal of improving oil spill forecasting (ASCE, 1996; Reed et al., 1999; Spaulding, 2017). These models have been developed from two-dimensional horizontal models to three-dimensional multiphase models, from considering only oil on the surface to oil distributed in multiple interacting phases, and from including a single environmental factor to atmosphere–wave–current coupled effects. Although these theories and data are valid, oil behaviour is complex, and many aspects of this behaviour are far from being clarified satisfactorily.

Currently, oil spill models incorporate a range of parameters, partly due to a lack of knowledge of the underlying mechanisms behind oil transport and reaction processes. Hodges et al. (2015) argued that empirical parameters are one of four major contributors to uncertainty in an oil spill model. Complicated environmental conditions and the complex mixture of hundreds of chemicals make every spill different, and determining a unique set of appropriate parameters for each event is impractical and difficult. For example, the 3% wind drift factor for oil movement considers average conditions, and the implication just represents average conditions and the actual factor ranges from 1 to 6%. Once submerged, oil particles driven only by water currents have a net lower drift speed than that assumed by the 3% rule. Moreover, oil converging in windrows accelerates, and the transport velocity becomes higher than the average 3%, and some variables, such as wind deflection angle, are disputed. Because an oil layer is too thin to experience the full Ekman spiral, the wind deflection angle has previously been set to zero (Coppini et al., 2011; Huntley et al., 2011). However, Samuels et al. (1982) argued that the veering angle is related to wind speed; when wind speeds are low, the average deflection angle can be as high as 20°.

Understanding the model structure and underlying principles is a key requirement for increasing model reliability. Parameter rationalities must first be widely accepted before model parameters can be optimised, and without extensive experimentation, a model using approximated parameters may not simulate satisfactory results. Although oil spill numerical results rely heavily on parameter rationality, near-optimal parameters have typically been estimated by manual calibration to match observations of real-world phenomena. However, because

* Corresponding author.
E-mail address: bren@dlut.edu.cn (B. Ren).

https://doi.org/10.1016/j.marpolbul.2018.07.026
Received 18 December 2017; Received in revised form 3 July 2018; Accepted 8 July 2018
Available online 20 July 2018

numerous parameters are related to oil movements, determining the most suitable ones is a time-consuming exercise that requires thorough experimental analysis.

Instead of obtaining universal parameters applicable to any condition, this study evaluated a method for seeking the most suitable parameters according to the location or event of interest. The genetic algorithm (GA) technique, inspired by the principles of biological evolution and natural genetics, has been widely adopted as an efficient tool for searching near-optimal solutions to nonlinear, nonconvex and multimodal problems (Gobeyn et al., 2017; Haupt and Haupt, 2004). Previous studies have demonstrated robust, modern approaches for employing GAs, which have been widely used in a variety of optimisation and search problems. However, few studies have employed GAs for optimising the parameter estimations of oil spill models.

When a GA is combined with an oil spill model under calibration, the model must be executed for a number of iterations; the computational bottleneck issue is no longer a limitation due to progress in computing equipment. Before GAs are implemented within oil spill modelling, an objective function evaluating the fitness of each model run should be provided in advance. Although there have been significant research advances in oil spill dynamics, the qualitative comparisons between simulation and observation is universal. At present, oil slicks on the sea surface can be accurately captured by observations from aerial images and satellites, which provide comprehensive evidence for the damage extent. Huntley et al. (2011) introduced two metrics for measuring simulation success: the percentage of the predicted spill area contained in the observed area and that of the observed polluted area contained in the simulated area. With the advent of fine-scale remote sensing techniques, an algorithm judging from scattered points to a whole plane seems more promising.

The purposes of this study are (1) to propose an objective function for the quantitative assessment of oil spill model performance and (2) to enhance model accuracy using of a GA. Following the introduction, Section 2 describes the basics of the oil spill model incorporating optimised design process. In Section 3, we apply the proposed model to the Dalian New Port accident that occurred on 16 July 2010. Section 4 presents the conclusions and applications of this study.

2. Methods

2.1. Environmental factors

Geographically, Dalian New Port is located on the boundary between the southern region of the Liaodong Peninsula and the North Yellow Sea (Fig. 1). It is a major seaport in North China, that has led to rapid economic growth in the region. However, this port has been affected by severe oil spills, including those from *Maya 8* in 1990, *Ya He* in 2001, *Arteaga* in 2005, and most recently, the Dalian New Port accident in 2010 (Guo and Wang, 2009; Guo et al., 2014; Xu et al., 2012). The Dalian New Port accident resulted in 35,000 t of crude oil being discharged into the coastal area on 16 July 2010, making this the largest marine oil spill in China's history. The spilled oil contaminated more than 300 km^2 of sea area and 80 km of coastline to varying degrees (Fig. 1(d)).

Oil spill behaviour is determined by the surrounding environment conditions as well as the physicochemical properties of the spilled oil; therefore, combining accurate environmental dynamic information is key for simulation accuracy. Hydrodynamic data (tides, currents and waves) to study oil spill behaviour were obtained from a wave–current coupled model. The current model in use is a semi-implicit Eulerian–Lagrangian finite-element (SELFE) model, which is a state-of-the-art, free-surface, primitive equation, hydrostatic model with Boussinesq and hydrostatic approximations (Zhang and Baptista, 2008). Considering that wave-driven current and wave breaking playing a significant role in spreading out oil slicks and propelling permeating oil droplets into the water column, wave data for this study were acquired from a third-generation wave model called the Simulating Waves Nearshore (SWAN) model (Booij et al., 1999), to solve transport equations of wave action density. Wave–current interactions occur over a wide range of both wave and current conditions; therefore, the SWAN model is iteratively two-way coupled to the SELFE model (Guo et al., 2016). Surface wind stress, bottom stress and radiation stress computed in SWAN model were provided to the SELFE model, and in turn, the SEFLE model offered current fields and water level elevation that were used in the SWAN model to calculate wave parameters for the next time step. The unstructured grid of the wave–current coupled model extended from Dalian New Port into the entire Bohai Sea and North Yellow Sea. The finest resolution occurred near Dalian New Port, with a grid spacing of approximately 20 m, and the resolution was relatively coarse, exceeding 1000 m, in areas far from the spill source (Fig. 1). The hydrodynamic model verification results were detailed in Guo et al. (2014). The maximum deviation of significant wave height from the measured values at the nearby monitoring location was within 0.2 m. The average root-mean-square error for water level simulation was less than 0.1 m, and the mean correlation coefficient of current speed between the observed and simulated values was over 0.9. Overall, the wave–current coupled model correctly reproduced the main hydrodynamic processes in the accident area waters and was capable of providing credible information for oil spill simulation.

Wind data, employed for wind driven currents, were acquired from re-analysis data based numerical results provided by the Weather Research & Forecasting Model (WRF) spanning 20°–52°N and 117.5°–152°E. Despite the fine temporal and spatial resolution of the WRF results (3-h time interval, and a horizontal resolution of 0.1° by 0.1°), the wind data used for calculating the oil particle trajectory were obtained from the records (1-h time interval) of a local meteorological station (Fig. 2), considering its vital role in determining spill trajectory accuracy. The region is characterised by a typical medium latitude monsoon climate, which consists of cold, dry winters and hot, wet summers.

2.2. Oil spill model

In this study, the fate and transport of spilled oil was governed by the advection under the actions of currents, wind, and surface waves; mechanical spreading of inertia, gravitational, surface tension and viscous forces; horizontal diffusion due to turbulence and shear effect; vertical entrainment and resurfacing; weathering processes such as evaporation, emulsification and dissolution; and the interaction of oil with the coastline (Fig. 3).

Considering the amount of oil released as a larger number of virtual particles that are tracked individually is an approach that has been widely adopted, and the model that employs this approach is known as the oil particle model. In this particle-based approach, oil spill movements are computed according to transport forced by advection (currents, winds, and surface waves) and turbulent diffusion. The advection velocity of an oil particle is computed as follows:

$$\vec{U}_a = C_{cr}\vec{U}_{cr} + C_{wind}D_{wind}\vec{U}_{wind} + C_{wave}\vec{U}_{wave} \quad (1)$$

where $\vec{U}_{cr}$ is the water current velocity interpolated from the hydrodynamic model; $\vec{U}_{wind}$ is the wind velocity 10 m above the water surface, C_{wind} is the wind drift factor, D_{wind} is a transformation matrix used to account for the wind deflection angle, $\vec{U}_{wave}$ represents the calculated wave Stokes drift, and C_{wave} is the wave drift factor.

The wind deflection angle is calculated as follows (Samuels et al., 1982):

$$\theta = D_a \exp(-10^{-8}U_{wind}{}^3/\nu g) \quad (2)$$

where ν is the kinematic viscosity of seawater. As opposed to its original form, the constant D_a is replaced by a variable.

$\vec{U}_{wave}$ represents the wave Stokes drift, calculated as follows:

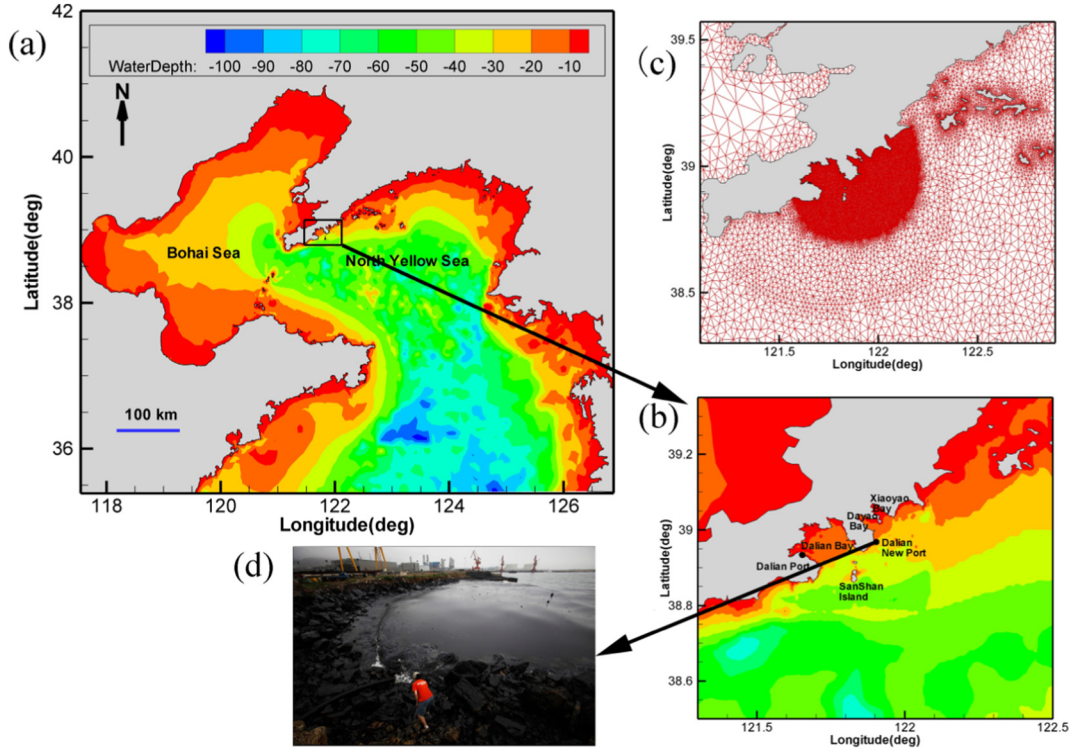

Fig. 1. Bottom topography of (a) the computational domain and (b) the Dalian coastal region near the spill site. (c) Triangle computational grid for the hydrodynamics model, with 81,697 nodes and 157,885 elements. (d) The coastal region near the spill site covered by the oil slicks.

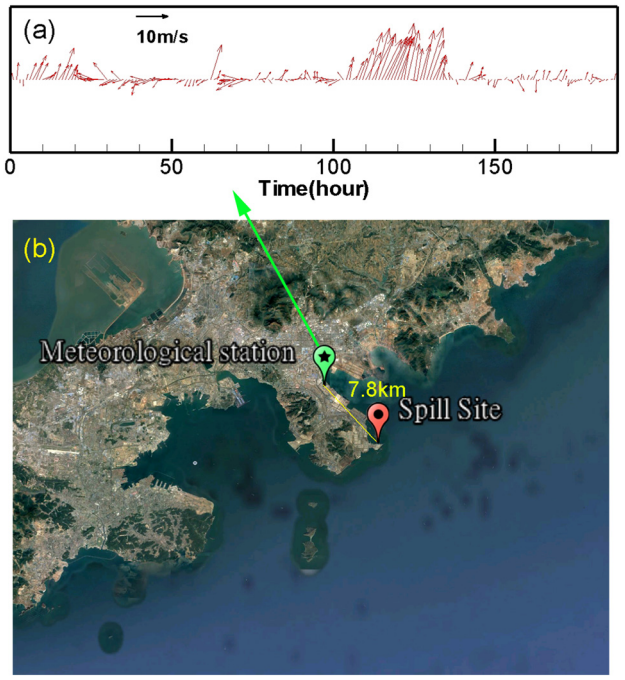

Fig. 2. (a) Time series of measured wind data (16 July 2010 to 23 July 2016). (b) Location of the meteorological station, which is 7.8 km from the spill site.

$$\vec{U}_{wave} = \frac{k\sigma H_s^2 \cosh(2kz_0)}{8\sinh^2(kh)} \tag{3}$$

where k is the wave number, ω is the angular frequency, H_s is the significant wave weight, and z_0 is the vertical position of oil particles measured upwards from the water surface.

Although the Stokes drift formula has been included in previous oil spill numerical models (Cucco et al., 2012; Guo et al., 2014), it should be noted that this formula is highly problematic for directly simulating sticky oil, as the Stokes wave theory is based on an inviscid fluid assumption. Therefore, we added a modified coefficient C_{wave} before the classical Stokes drift velocity.

In addition to the determinate advective movements, oil droplets experience random diffusion due to turbulent fluctuations. Turbulent diffusive transport is calculated by a random walk procedure with a horizontal diffusion coefficient. Based on a previous study (Chao et al., 2003), the diffusive distance ΔS can be expressed as follows:

$$\Delta S = [R]_0^1 \sqrt{12 D_h \Delta t} \tag{4}$$

where Δt is the time interval, $[R]_0{}^1$ is the evenly distributed random number in the interval 0 to 1, and D_h is the horizontal diffusion coefficient. Chao et al. (2001) selected D_h as a constant, whereas other models obtained the horizontal diffusion coefficients from the Smagorinsky formula (Guo and Wang, 2009; Korotenko et al., 2004).

As subgrid-scale turbulent diffusion is caused by the hydrodynamic stability of sheared currents at high Reynolds numbers, the latter method was more applicable. Hence, we adopted the Smagorinsky formula to acquire diffusivity D_h:

$$D_h = C_t l^2 \left[\left(\frac{\partial u}{\partial x} \right)^2 + \left(\frac{\partial v}{\partial x} + \frac{\partial u}{\partial y} \right)^2 / 2 + \left(\frac{\partial v}{\partial y} \right)^2 \right]^{1/2} \tag{5}$$

where l is a characteristic length and C_t is an empirical constant that requires artificial assignment.

Spreading is the horizontal expansion of an oil slick due to mechanical forces such as inertia, viscosity, gravity, and interfacial tension. The inclusion of a traditional spreading algorithm developed by the classical Fay's theory may lead to uncertainties (Yapa, 2005), if we assume that a thick slick can feed oil into a thin layer, especially during the first stage of a spill. In our model, spreading was regarded as a diffusion process and simulated with the random walk method.

The diffusion-like spreading coefficient D_{sp} is calculated using the following equation (Mackay et al., 1980):

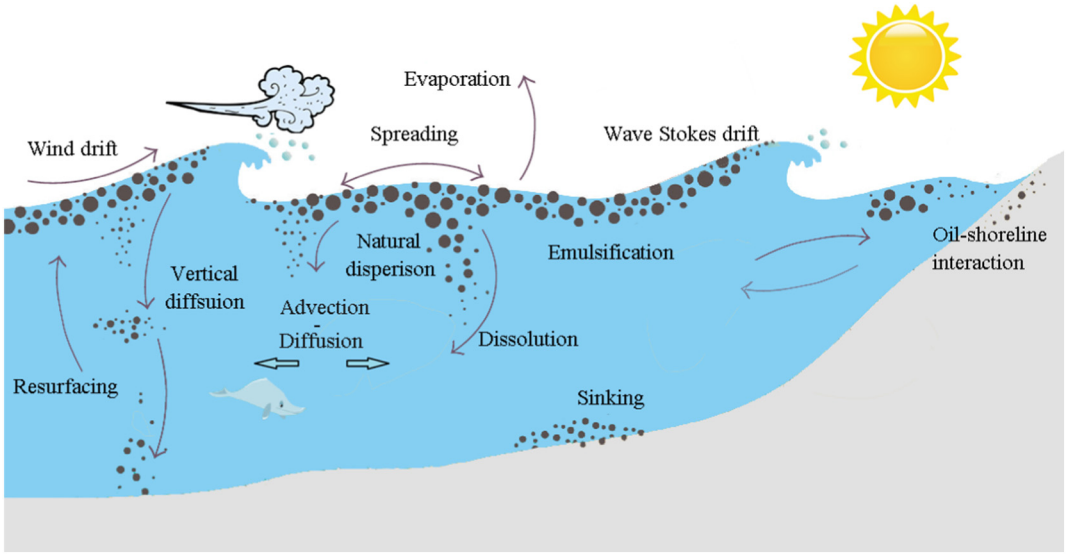

Fig. 3. Schematic description of oil spill processes.

$$D_{sp} = K_s \frac{\Delta^{1.6} g V^2}{\nu_w^{1/6}} \tag{6}$$

where $\Delta = (\rho_w - \rho_o)/\rho_w$, ρ_w and ρ_o are the sea water and oil densities, respectively, V is the volume of spilled oil, ν_w is the sea water kinematic viscosity, and K_s is the empirical constant. The spreading process ceases when an oil-specific terminal thickness T_t is reached; this thickness is assigned different values based on oil properties (Reed, 1989).

When a slick becomes too thin, it can be split by shear currents and wave forcing, and some oil particles may be dispersed into the water column by the breaking waves. This process is called natural dispersion and mainly depends on the wave energy environment. The rate of oil entrainment from the surface to the subsurface λ_{ow} can be scaled as follows (Tkalich and Chan, 2002):

$$\lambda_{ow} = \frac{k_e \omega \gamma H_s}{16 k_i L_{ow}} \tag{7}$$

where k_e is the coefficient obtained from experiments, ω is the wave frequency, γ is the dimensionless damping coefficient, k_i is the coefficient concerning the mixing depth of the individual particles and L_{ow} is the vertical length-scale parameter depending on the type of breaking wave.

The intrusion depth z_i that the oil droplet may penetrate is computed as follows (Delvigne and Sweeny, 1988):

$$z_i = (k_i + b_i^* [\mathrm{R}]_{-1}^{1}) H_s \tag{8}$$

where b_i is the amplitude of intrusion depth and $[R]_{-1}^{1}$ is the uniform random number between -1 and 1.

The horizontal movements of subsurface oil particles are analogous to those of surface oil particles except in the case of direct wind drag. The Langeven equation is used to calculate vertical particle velocity using stochastic perturbations from the Markov chain for deceleration (Lonin, 1999):

$$\frac{dZ}{dt} = w + w_o + w' \tag{9}$$

where Z is the particle vertical coordinates, w is the background flow velocity interpolated from the hydrodynamic model, w_o is the rising velocity due to buoyancy, and w' is the turbulent fluctuations.

When an oil particle reaches the shoreline, it may be beached. Once stranded along the shoreline, it may also re-enter the water. Two important parameters, oil-holding capacity and return probability, are defined to quantify the interaction of oil particles with the shoreline.

The maximum beach capacity $Q_{\max}$ is given by Humphrey et al. (1993):

$$Q_{\max} = L_s W_s D_s \eta_{eff} \tag{10}$$

where L_s, W_s, and D_s are the length, width, and depth of sediments on the beach, respectively; and η_{eff} is the effective porosity of sediments on the beach.

The return probability P_r from the shoreline to the water can be computed as follows:

$$P_r = 1 - 0.5^{t/\lambda} \tag{11}$$

where λ is the half-life of particles remaining on the shoreline. A random number between 0 and 1 is assigned to each deposited particle, and particles with a random value of less than P_r will return to the sea.

An accurate prediction of changes in the physical and chemical properties also provides necessary information for improving slick trajectory forecasting. For example, the formation of stable water-in-oil emulsions combined with the evaporation of lower molecular weight hydrocarbons leads to a sharp increase in viscosity. In this model, three main early-stage weathering processes, namely evaporation, emulsification and dissolution, were integrated to predict their combined effects on the physicochemical properties of spilled oil. The numerical algorithms are provided in detail in Guo et al. (2014).

2.3. GA algorithm for optimisation

In the oil spill model, 11 kinetic parameters required calibration before model application (Table 1). Compared with traditional optimization methods based on the gradient of a function, the GA technique is more appropriate for solving multiple parameter estimation problems where the objective function responses contain multiple optima. GAs originate from a binary GA, but continuous GAs can solve a problem where the variables are continuous and have real values. In order to avoid time-consuming manual calibration, we resorted to continuous GA to determine suitable parameters, improving on the time-consuming manual method.

Prior to GA implementation, a fitness function must be assigned, which measures the model performance for oil spill simulation. Existing oil spill models do not equip an algorithm for quantitatively evaluating model performance. Although the reliability of some oil spill models can be verified by comparing the concentration of petroleum hydrocarbons at surveillance sites, it is debatable whether the model validation results are guaranteed for the whole region.

Oil slick extent on the sea surface reflects its spatial distribution

Table 1
Model parameters to be optimised and their variation ranges.

Parameter definition	Symbol	Corresponding equation	Unit	Variation range
Current factor	C_{cr}	(1)	–	0.9–1.2
Wind drift factor	C_{wind}	(1)	–	0.01–0.06
Wind deflection angle	D_a	(2)	°	5–25
Stokes drift factor	C_{wave}	(1)	–	0.5–2.0
Empirical coefficient on diffusivity	C_t	(5)	m^{-1}	0.05–10
Spreading parameter	K_s	(6)	–	1–100
Entrainment coefficient	k_e	(7)	–	0.1–0.8
Intrusion depth coefficient	K_i	(8)	–	0.5–2.5
Amplitude of intrusion depth	b_i	(8)	–	0.1–1.0
Effective porosity of the beach	η_{eff}	(10)	–	0.1–0.6
Half-life of particles on the beach	λ	(11)	h	1–100

characteristics and is easily obtained, making it a key indicator for oil spill models. Integrating the two metrics by Huntley et al. (2011), we define a function P_{op} for measuring model success:

$$P_{op} = w_1 \frac{S_{os}}{S_o} + w_2 \frac{S_{os}}{S_s} \tag{12}$$

where S_o is the actual area covered by slicks, S_s ris the sea surface area polluted by numerical oil particles, S_{os} is the superposition of the observed and simulated areas, and w_1 and w_2 are the weighting factors, where $w_1 + w_2 = 1$. When the predicted coverage is sufficiently small to be entirely enclosed by the observed area, S_{os}/S_s is 1 but S_{os}/S_o may be much less than 1. In contrast, if the predicted oil film covers all actual slicks but most areas are mis-identified, S_{os}/S_s approaches 0. For an ideal simulation result, P_{op} equals 2, indicating that all true contaminated areas are predicted, and no clean sea surface is mistaken for a contaminated area. A perfect simulation is not common, and therefore a straightforward approach to the multi-objective optimisation problem is to weight each function and add them together (Haupt and Haupt, 2004). A chromosome is created that holds parameter values for the oil spill model solution and the specific fitness of this solution.

The slick polluted area is the integral of each discrete computational element invaded by oil particles. We assigned a value of 1 to the presence of a computational element in either observation (O) or simulation (S) and a value of 0 to its absence, and a matrix of four possible states resulted (Table 2) as noted by Aronica et al. (2002).

Eq. (12) was subsequently redefined as follows:

$$P_{op} = w_1 \frac{\sum_{i=1}^{ne} A_i P_i^{O_1 S_1}}{\sum_{i=1}^{ne} A_i P_i^{O_1 S_0} + \sum_{i=1}^{ne} A_i P_i^{O_1 S_1}} + w_2 \frac{\sum_{i=1}^{ne} A_i P_i^{O_1 S_1}}{\sum_{i=1}^{ne} A_i P_i^{O_0 S_1} + \sum_{i=1}^{ne} A_i P_i^{O_1 S_1}} \tag{13}$$

where P_i^{O1S1} takes a value of 1 for element i, where oil slick is absent in both observation and simulation. P_i^{O1S0} and P_i^{O0S1} are assigned a value of 1 respectively for an element where the oil particle is present in the observation and absent in the simulation, and an element where the oil particle is absent in the observation and present in the simulation. A_i is the area of element i, and ne is the number of elements.

Table 2
Matrix of observation/simulation combinations for a binary classification scheme.

	Absent in simulation (S_0)	Absent in simulation (S_1)
Absent in observation (O_0)	O_0,S_0	O_0, S_1
Present in observation (O_1)	O_1, S_0	O_1, S_1

The detailed implementation steps of the GA were presented as follows:

1. Generate an initial population of N_{pop} candidate chromosomes (N_{pop} = 100 in this study). The simplest way in which to create the initial population is to generate random strings from a uniformly distributed random real number in the specified range of each parameter.

2. Execute the oil spill model N_{pop} independently with the parameters in the chromosome. Calculate the fitness F_i of each individual chromosome according to Eq. (13).

3. Employ truncation selection, wherein the fittest 50% of the population has a chance of reproducing. Adopt a roulette-wheel algorithm to assign a probability of reproduction based on each individual's fitness, with relatively larger fitness values being assigned a higher probability.

4. Mate two parents to create two offspring. Select a random position to cut both parent number strings; form one offspring by taking the fragments before the cutting position of parent A and after the cutting position of parent B, and vice versa, to produce the second offspring. Appearance of the swap point anywhere in the chromosome indicates that the crossover rate is 1. Repeat mating until the offspring number equals N_{pop}.

5. Mutation occurs with a uniform probability p_{mut} (p_{mut} = 0.1). For every gene of an offspring chromosome, generate a random number R_{mut} between 0 and 1; mutation occurs only if $R_{mut} \leq p_{mut}$. Replace the targeted gene to a random value within the designated variation range.

6. The replacement operator is overlapping, i.e. once N_{pop} offsprings have been produced, the entire parent population is wiped out and replaced by the offspring population. The elitism strategy is adopted to guarantee that the genotype of the fittest individual will be passed on intact to the next generation. The new population thus becomes the current population. Repeat step 2 until the pre-determined number of generations is achieved.

Fig. 4 presents the entire linking process of the oil spill model with the GA optimiser. The role of the hyper-parameters in enhancing calibration performance is no less than that recommended by Gibbs et al. (2008).

3. Results and discussion

3.1. GA versus empirical parameters

On 16 July 2016, a fire disaster in Dalian New Port led to a pipeline releasing approximately 35,000 t of crude oil into nearby fiords and the Yellow Sea. This event is the largest accidental marine oil spill in the history of China, which devastated the surrounding environment and resulted in huge economic losses. The GA technique was used to simulate the spilled oil trajectory and distribution during the first week after the Dalian New Port oil spill in 2016.

As some empirical parameters have been adopted in previous studies, they may also be directly applied to oil spill models (ASCE, 1996; Reed et al., 1999; Spaulding, 2017). The merit of the GA is that humans do not perform the calculations; the model parameters are searched by optimization in a certain domain. We evaluate whether the GA can produce better results than those obtained using experimental data. Firstly, we employed empirical parameters from previous research (Table 3) to simulate the oil spill in Dalian New Port (Exp. 1). Then, with the purpose of simulating oil patterns close to the observed aerial image at 01:00 on 29 July 2010, the GA was coupled with the numerical oil spill model (Exp. 2). Initial parameters were generated in the assigned variation range. The simulated surface slick distributions based on two groups are shown in Fig. 5(a) and (b), respectively.

The observed slick boundary enclosed an area of 16.6 km^2. The polluted area obtained using empirical parameters (Exp. 1) was 18.7 km^2, 10.8 km^2 of which overlapped with the observed area. With respect to simulated droplets, 42.2% were scattered outside the true slick outline, and some extended 5 km from the boundary. The fitness

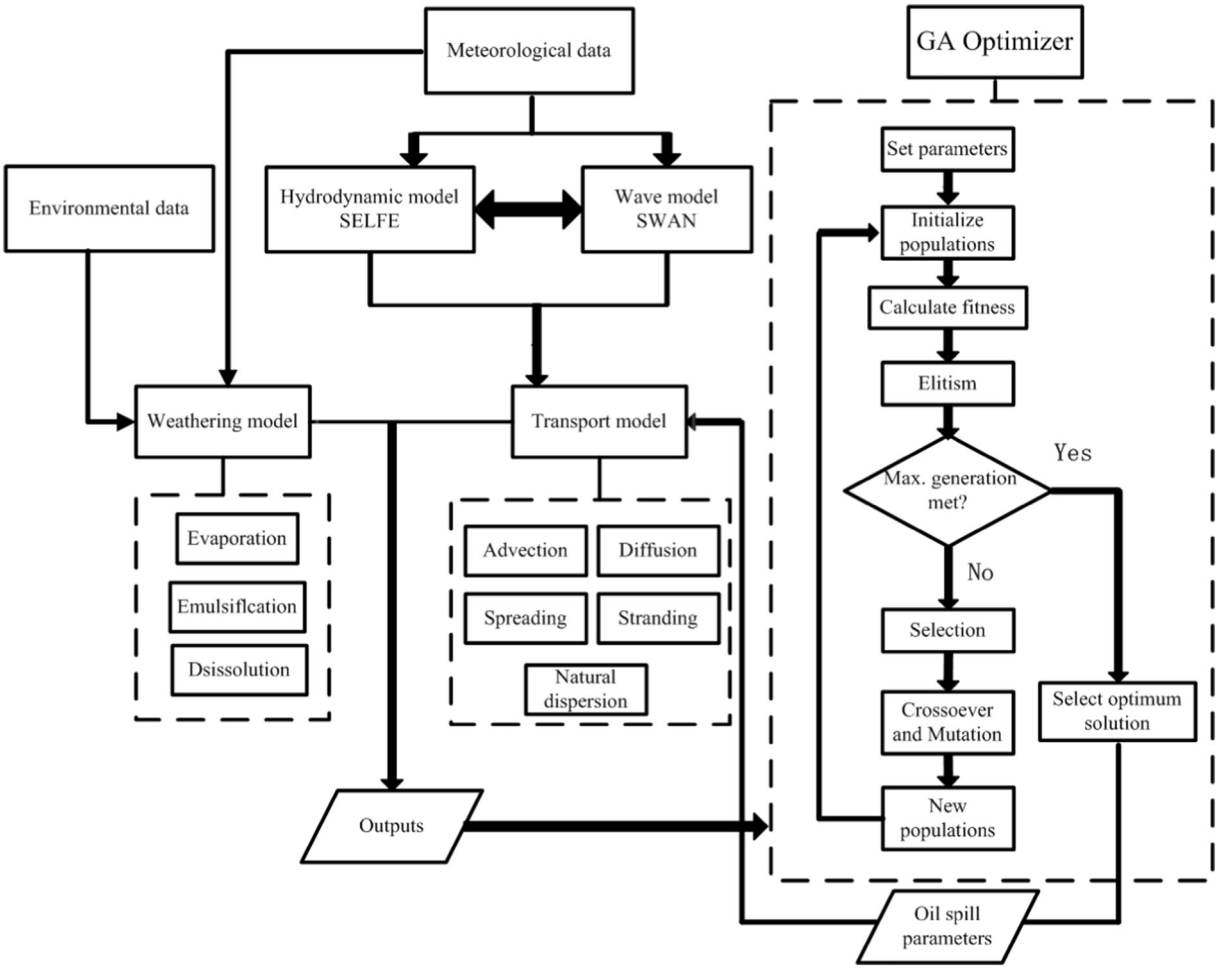

Fig. 4. Flow chart of the oil spill model linked with the GA optimiser.

Table 3
Parameter values of each experiment.

Parameter symbol	Exp. 1	Exp. 2	Exp. 3	Exp. 4	Exp. 5	Exp. 6	Exp. 7
C_{cr}	1.0	1.021	1.013	1.006	0.925	0.933	0.929
C_{wind}	0.03	0.032	0.033	0.033	0.041	0.037	0.038
D_a	15.0	6.88	5.31	6.34	9.76	7.15	7.52
C_{wave}	1.0	1.017	1.136	1.125	1.689	1.638	1.622
C_t	1.0	0.151	0.169	0.174	0.385	0.368	0.361
K_s	10	85.6	81.8	80.3	51.7	60.2	55.3
k_e	0.2	0.263	0.252	0.248	0.352	0.305	0.319
K_i	1.5	1.478	1.512	1.512	1.518	1.649	1.885
b_i	0.5	0.236	0.235	0.256	0.233	0.220	0.212
η_{eff}	0.3	0.216	0.224	0.232	0.351	0.376	0.368
λ	24	22.5	25.1	26.5	46.2	35.7	36.4

value of this run was only 0.614, indicating that the estimated parameter values were sub-optimal for estimating the oil spill observation. In terms of the results of the model incorporating GA, the best fitness value of the first random generation was only 0.185. However, the best fitness value of the 72nd generation exceeded that of Exp. 1. Despite its initial poor performance, the GA improved model performance to that achieved by using empirical parameters. After 100 generations, the simulated area reached 17.8 km^2, 12.3 km^2 of which lay in the observed slick boundary. The best individual fitness value is 0.716 (Fig. 6), which showed better, but not perfect, agreement with the observations.

The fitness value of 0.716 using the GA suggested that there is further scope for improvement. A simple approach would be to extend model evolution to more generations at the expense of computation time. An alternative, more feasible solution would be to take full advantage of the empirical parameters from previous studies. In Exp. 3, an individual chromosome carrying pre-specified parameters, used in Exp.1, was inserted into the first-generation population, and other initial individuals were still generated at random within the variation range. The subsequent process was the same as that for Exp. 2. The use of elitism artificially guarantees that the best individual in the next generation is at least not as bad as its elder generation. The objective function value started at 0.614 and ended at 0.853 through 100 generations of evolution (Fig. 6), representing an 18.5% increase compared with evolution without using high-quality origin. The evolution speed was also faster compared to that relying solely on computer-generated ancestors. The simulated oil slick pattern is shown in Fig. 5(c), and the simulated particles were mostly limited within the observed slick boundary. Thus, it was clear that calibration starting from relatively reliable empirical parameters could produce more accurate results in equivalent generations.

3.2. Weighting factor selection

So far, we had assumed that the two weighting factors were identical. For a multi-objective optimisation problem, the goal is to approximate the Pareto-optimal trade-offs between conflicting objectives (Nicklow et al., 2010). The most straightforward approach to multi-objective optimisation was to weight each function and add them together, where the key task was determining appropriate weighting values. However, it was not possible to judge the relative weight of the two cost functions in Eq. (12) prior to running the GA. Therefore, 10

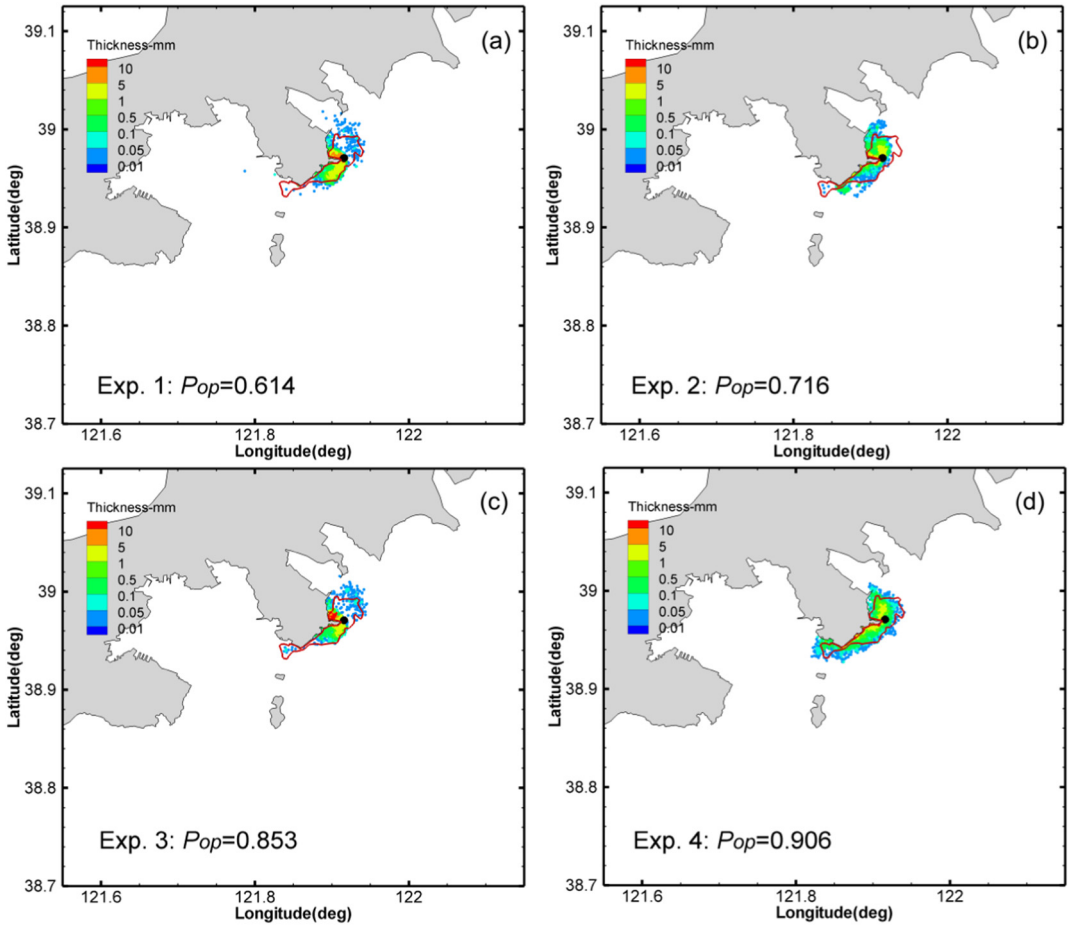

Fig. 5. Simulated oil spill distribution shown as Lagrangian particles, and the observed oil slick outline on the water surface (red line) at 01:00, 18 July 2010: (a) simulated directly based on empirical parameters, (b) simulated using the GA from random individuals, (c) simulated using the GA and empirical parameters (w_1 = 0.5), and (d) simulated using the GA (w_1 = 0.6). (For interpretation of the references to colour in this figure legend, the reader is referred to the web version of this article.)

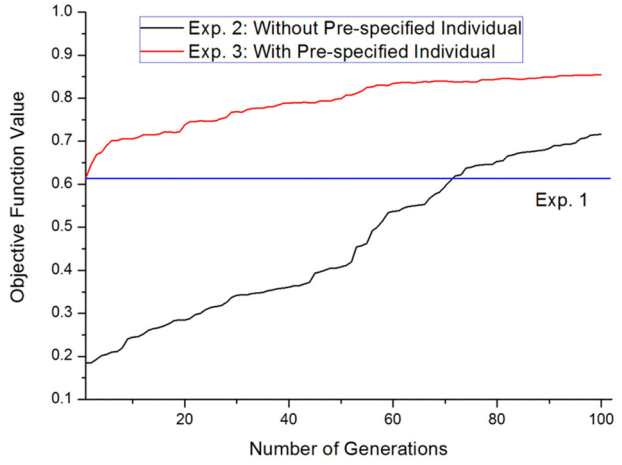

Fig. 6. Best-so-far objective values for the oil slick simulation at 01:00, 18 July 2010. Solid blue line represents the performance based on manual setting parameters without using the GA. (For interpretation of the references to colour in this figure legend, the reader is referred to the web version of this article.)

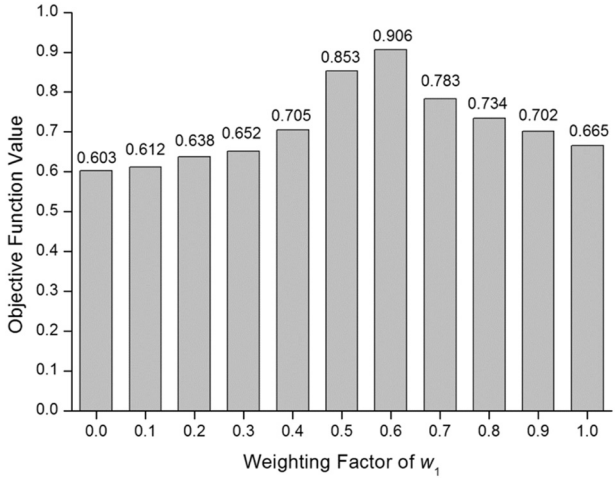

Fig. 7. Model performance with various weighting factors.

independent oil spill runs were conducted with varying w_1 uniformly distributed from 0 to 1. The weights were multiplied by the cost value and added together to obtain a single object value, which the GA then maximised. As shown in Fig. 7, there were clear differences between the final fitness values using various weighting factors. If the only purpose was to meet w_1 = 0 or w_1 = 1, the model performance was quite poor. The objective value initially increased and then decreased as the weighting factor increased, with a peak value appearing at w_1 = 0.6 (Exp. 4). The final fitness values range from 0.603 (w_1 = 0.0) to 0.906 (w_1 = 0.6). The weighting factor modulation yielded more reliable results to some extent, as shown in Fig. 5(d). Hence, the objective fitness values were calculated according to w_1 = 0.6. While this weight

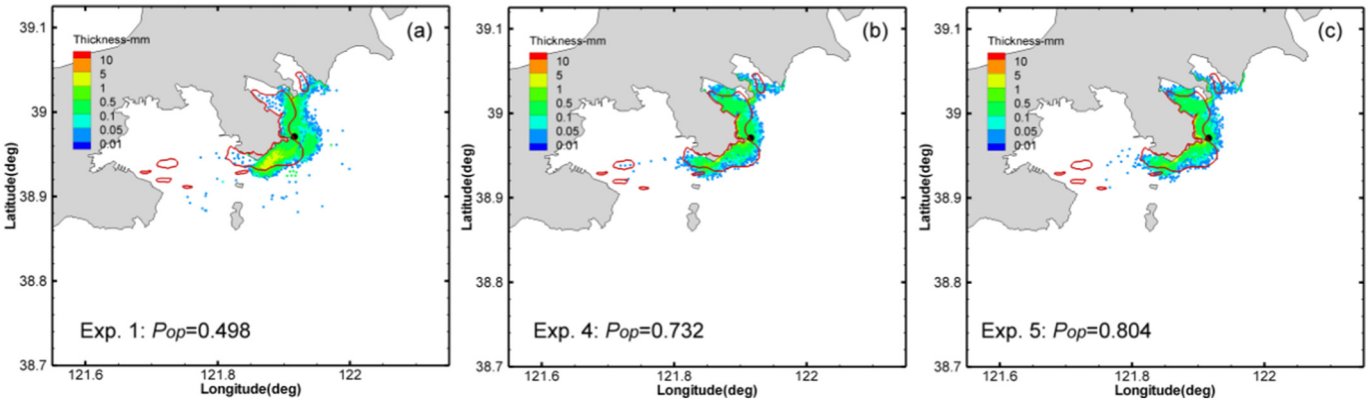

Fig. 8. Oil slick distribution on the sea surface observed from aerial image (red line) and simulated by the numerical model (coloured shading) at 06:00, 20 July 2010. (For interpretation of the references to colour in this figure legend, the reader is referred to the web version of this article.)

allocation may not be appropriate for other oil spills, it can easily be adjusted to seek suitable weighting factors for each new accident of interest.

3.3. Validation with optimised parameters

The parameter estimation process was performed for the period from 19:00 (GMT + 08:00) on 16 July 2010 to 01:00 on 18 July 2010. After obtaining near-optimal parameters, we attempted to take advantage of them to predict subsequent oil slick trajectories. Motivated by the simulation of spilled oil distribution at 01:00, 18 July, we proceeded to simulate the oil slick patterns. Fig. 8 demonstrates the surface oil slicks obtained numerically and observed from aerial image (06:00 on 20 July 2010).

The similarity between the simulated patterns and observed images was poorest using manual setting parameters without the aid of the GA (Exp. 1). Nearly half the predicted slicks are located beyond the extent of observation (Fig. 8(a)), and the fitness value is only 0.498. When the GA is adopted (Exp. 4), the simulation result is improved with an objective function of 0.732 (Fig. 8(b)).

The same set of parameters resulted in a P_{op} value of 0.906 at 01:00 on 18 July, but only 0.732 at 06:00 on 20 July, suggesting that parameter effectiveness decreases with time, which was expected based on this dataset. We used the numerical model with this set data to simulate the oil slick distribution for 21 July (Fig. 9(a)). After 4–5 days, as the oil slicks broke into smaller droplets and became progressively thinner, the oil films may have been dispersed more rapidly than before. The estimated polluted area increased to 225.5 km^2 by 12:00 on 21 July, according to the temporal aero-picture. An area of 81.3 km^2 inside the observed slick outline was not covered by the oil particles, and the fitness value was only 0.476. When we employed the GA to directly optimise the oil distribution at 06:00 on 20 July (Exp. 5), the last generation fitness value was 0.804 (Fig. 8(c)). For the oil spill model run at 12:00 on 21 July and using these obtained parameters, the function P_{op} value was 0.636. This indicated that better performance was acquired when more recent slick distribution information was utilised.

Next, we ran the oil spill model to simultaneously optimise oil slick simulations at two different moments: surface oil slicks at 12:00 on 18 July and 12:00 on 20 July. The objective functions were formulated by assigning homogeneous weights (Exp. 6) and heterogeneous weights (Exp. 7) to distinct moments. The array of weights followed the principle inverse interval to a power, i.e. the latecomer receives a greater weight. For the strategy adopting unequal weights, the weighting factor was set to 0.3 for 18 July and 0.7 for 20 July. When both obtained sets of data are applied to predict oil film distributions at 12:00 on 21 July, we found that both areas predicted to be polluted by oil particles were generally in agreement with the observations. Quantitatively, the method with varying weights produced a more reliable forecast (P_{op} = 0.788) than the other method did (P_{op} = 0.715), indicating that the proximity principle worked. Since forecasting errors increase with time, a greater reliance on the latest slick information is advisable.

3.4. Discussion of model parameters

An improved understanding of parameters, as well as their contributions to model performance, is a primary purpose of modelling. In extreme instances unreasonable parameters may occasionally create results beyond expectations, whose improper usage by other modellers can cause problems. Hence, it is necessary to identify the optimal results from optimisation methods.

Both manually set and optimum values according to the GA are listed in Table 3. The variation range of C_{cr}, C_{wind} and K_i were less than 1% of the mean, implying that the margin of error was small. This explained how approximated parameters yielded acceptable forecasts. As for C_t, the maximum was more than twice the minimum, indicating that it should be calibrated for each case according to a variety of complex sea states. A greater uncertainty was also reflected in parameters characterising oil–shoreline interactions, owing to the limited experimental/observation data and the oversimplified approach.

It is often assumed that oil floats with the surface current at 100% of the current speed (ASCE, 1996; Chao et al., 2001). However, other values for the oil–water speed ratio do exist. Shen and Yapa (1988) found that a value of 1.1 can best account for the contribution of oil film drift floating at the water surface due to the current. This factor varied between 0.925 and 1.021 in our model, meaning that the widely-used value of 1.0 is workable but not precise in most cases. We set the final value at 0.929, slightly less than 1.0, which could be attributed to a slower water surface speed due to the presence of sticky slicks, whose damping effect are not typically considered.

Another critical parameter, the wind drift factor, was chosen as 0.038, falling at the high end of the range from 0.025 to 0.044 (ASCE, 1996). Although the 3% rule is one of the best-known rules in oil spill modelling, it only represents average conditions. The actual factor varies from 1 to 6%, depending on the spatial position of oil particles. The reason why this factor was slightly larger in our model may be that the wind data were measured on land (Fig. 2(b)), which was approximately 20% less than that likely to be measured at sea. The underestimated wind speed was compensated for by an enhanced wind drift weight. The other wind effect involved the deflection angle, which rotates approximately 20° clockwise to account for Coriolis effects in the northern hemisphere. This effect was neglected by Coppini et al. (2011) and Huntley et al. (2011), who considered that a slick on the sea surface was not subject to the full Ekman spiral. In our model, the D_a value was 7.52°, suggesting that the wind deflection was not likely to be over 7.5°, which met observational surface oil drift evidence in the

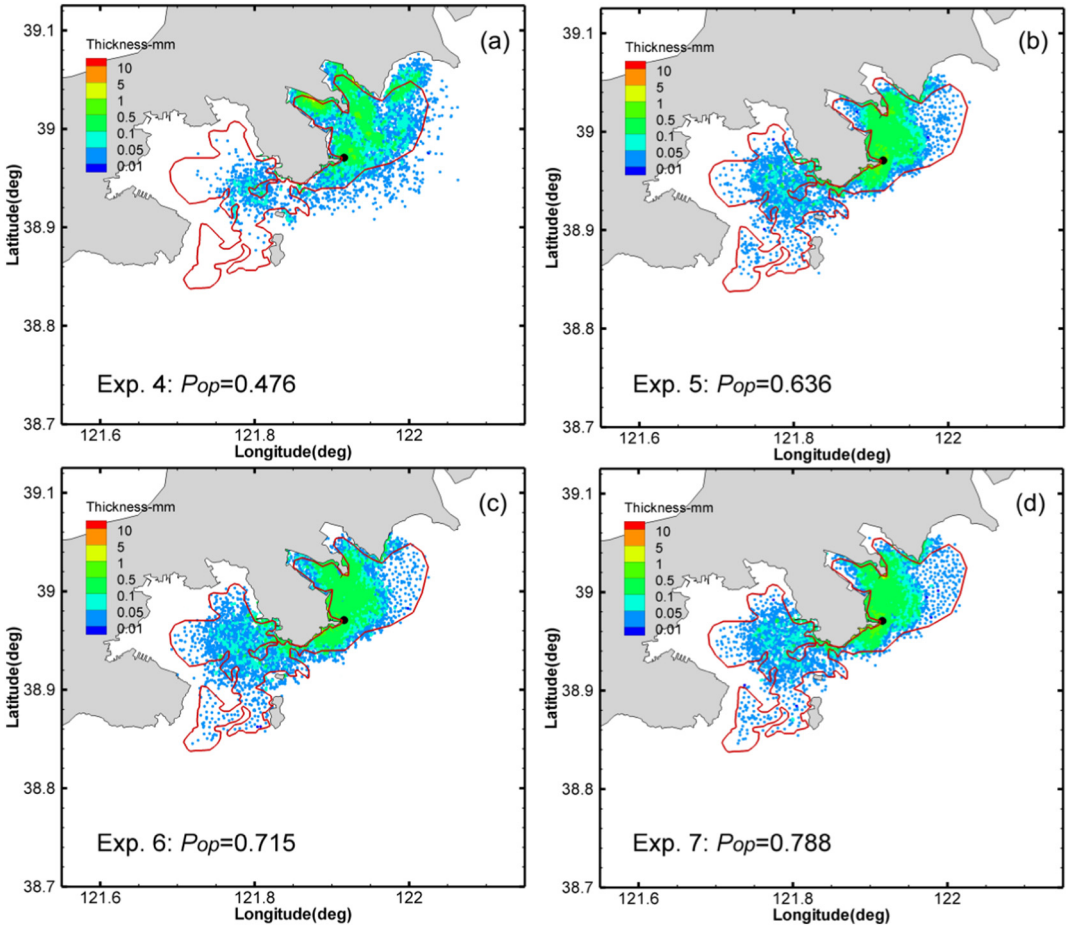

Fig. 9. Oil slick distribution on the sea surface observed from aerial image (red line) and calculated by the numerical model (coloured shading) numerical model at 12:00, 21 July 2010. (For interpretation of the references to colour in this figure legend, the reader is referred to the web version of this article.)

Arabian Gulf (Proctor et al., 1994). The value obtained in this study was far lower than that of 25° recommended by Samuels et al. (1982), further supporting the arguments of Coppini et al. (2011), Huntley et al. (2011), and Le Hénaff et al. (2012). A phenomenon whereby the current moves at an angle to the wind requires constant wind speed lasting over 24 h. The wind data interval was only 1 h, and this shifting effect was therefore non-distinctive. The frequent change of wind does not permit full development of the deflection angle. That the value is non-zero implies that the rotation effect does not disappear completely, partly due to the slick-enhanced viscosity forces.

It is suggested that small oil fragments are carried partly by the Stokes drift generated in the upper layer in response to wind waves and ocean currents. Stokes wave theory is only valid for an inviscid fluid and makes little sense for a sticky oil slick. Hence, choosing the coefficient C_{wave} 1.0 for the Stokes drift formula is inappropriate. Phillips (1977) assumed that a patch of oil slick moves faster than sea water elements by three quarters of the Stokes drift. The value of 1.622 was in close agreement with Phillips' estimate, and the difference may result from the overestimation of the weight data from the SWAN model without consideration of dissipated effects on waves by the oil slick.

Horizontal diffusivity, a dominant influence on oil transport simulations, has been measured in previous studies (Matsuzaki and Fujita, 2017). However, its value varied within the range of 1–100 $m^2 s^{-1}$ under external factors such as random waves or currents (ASCE, 1996), and it was unclear how best to estimate the horizontal diffusivity of oil. Although some constant values for the turbulent diffusion coefficient in oil-spill cases have been successfully estimated (Chao et al., 2003; Murray, 1972), it should be confirmed that they are more credible by using the Smagorinsky formula, because the gradient of velocity leads to effective diffusion in the horizontal direction. With the GA, we determined a C_t value of 0.361 m^{-1}, which resulted in a D_h of approximately 5 $m^2 s^{-1}$. This value was smaller compared with that in previous reports. It is typical for the simulation to focus on the 5 days after the spill, i.e. the early stages of oil slick transformation. Okubo (1971) derived a 4/3 power law between the apparent diffusivity and the scale of diffusion, and the superdiffusive transport phenomenon of the oil slick does exist (Guo et al., 2009). The diffusion coefficient increases with time, so that larger values appear in the long-term simulation.

The spreading coefficient K_S was 55.3, implying that, when the film thickness changed by 1 mm every 100 m in the horizontal direction, the velocity induced by thickness gradients was approximately 0.1 $m s^{-1}$. Spreading is an important process where a thick slick concentrated in a small area feeds a thin one occupying a larger area, and the rate weakens rapidly with distance from the release source. The slick is presumed to cease spreading when it becomes thinner than a terminal thickness of, for example, 0.1 mm (Reed et al., 1999). According to the spreading coefficient obtained in this study, this assumption is rational.

The entrainment coefficient k_e was estimated to be 0.319 from an initial value of 0.2. It is accounted for explicitly by intense wave dissipation through breaking in the nearshore waters. The intrusion depth coefficient of 1.217 was slightly smaller than the experimental value of 1.5 recommended by Delvigne and Sweeny (1988). Considering that dispersion processes correlated with oil physicochemical properties, slick thickness, and turbulence intensity, we assumed that this value was within acceptable levels. The complex sea state and varying weathering degrees resulted in a wider range of variation than the laboratory measured value of Delvigne and Sweeny (1988).

Due to the discharge source near the coastline, interactions between

spilled oil and the shoreline were evitable, which are highly complex and incompletely understood. The model assigned the maximum beach capacity and half-life of oil particles deposited on the beach. The effective porosity of the beach η_{eff} was 0.368, and the half-life time λ was 36.4 h. These two values were slightly larger than expected, because the main coast of Dalian New Port is primarily bedrock. One possible explanation is shoreline cleanup. Recovery operations were quickly launched after the oil spill to minimise the scale of the affected area and damage to environmentally sensitive resources. One of the protection methods laid multiple synthetic sorbent sheets along the shoreline to prevent oil returning into the water, which can adsorb up to 30 times their own weight.

4. Conclusion

An approach combining an oil spill model and the GA technique was presented to enhance prediction accuracy for a real oil spill event. First, a simplified criterion for assessing oil spill model performance was proposed, which was then maximised through a GA. Compared with results from manual methods, oil spill forecasts were better simulated using parameters obtained by the GA.

The major conclusions of this study are as follows:

(1) The proposed formula related to polluted area overlap ratio remedies the limitations of conventional oil spill models, which lack quantitative evaluation measures. Equipped with versatile weights, the equation was fully applicable to diverse scenarios.

(2) The GA could determine suitable parameters that resulted in good performance of the oil spill transport model, which was distributed within a reasonable range rather than simply subjectively determined. To deal with information from multiple moments, i.e. a multi-objective optimisation, we adopted the principle of proximity, whereby data obtained at a later time were given more weight. Recent improvements in oil spill data acquisition ensured that sequential data were available; therefore, this principle is highly practical.

(3) Some parameters, such as the wind drift factor and turbulent diffusion coefficient, were sensitive, indicating that they should be calibrated for each specific oil spill event, thereby avoiding an over-dependence on rules representing average conditions. In this way, our method could determine the most suitable parameters according to each location or event of interest.

Even though the GA could find suitable parameters for predicting oil spill trajectories, both basic experiments and real-time data acquisition under actual sea conditions are indispensable, not only for dependable parameter verification but also for providing excellent original values for optimisation. Some novel algorithms on oil spill processes are still required, such as the horizontal diffusivity formula presented by Matsuzaki and Fujita (2017), which can be used to depict diffusivity increases with diffusion scale.

In future research, the proposed method for evaluating model performance should be extended to include other oil spill behavioural data, such as hydrocarbon concentrations, to achieve more comprehensive oil spill trajectory and fate prediction. Furthermore, the oil spill modelling uncertainties may arise from inaccuracies in the environmental data used, and the GA is also employed to improve the precision of the meteorological and hydrodynamic models. Recent advancements in GA technology, such as the aggregation hybrid genetic algorithm, can be introduced to handle the multi-objective optimisation problem more effectively.

Acknowledgment

This research is sponsored by National Natural Science Foundation of China (Nos. 51609029, 51609168 and 51709140), Fundamental Research Funds for the Central Universities (3132018176), Liaoning Province Natural Science Foundation (20170540096), and the Key Laboratory of Water–Sediment Sciences and Water Disaster Prevention of Hunan Province, China (No. 2016SS02).

References

Aronica, G., Bates, P.D., Horritt, M.S., 2002. Assessing the uncertainty in distributed model predictions using observed binary pattern information within GLUE. Hydrol. Process. 16 (10), 2001–2016.

ASCE Task Committee, 1996. State-of-the-art review of modeling transport and fate of oil spills. J. Hydraul. Eng. 122 (11), 594–609.

Booij, N., Ris, R.C., Holthuijsen, L.H., 1999. A third-generation wave model for coastal regions 1. Model description and validation. J. Geophys. Res. Oceans 104 (C4), 7649–7666.

Chao, X., Shankar, N.J., Cheong, H.F., 2001. Two-and three-dimensional oil spill model for coastal waters. Ocean Eng. 28 (12), 1557–1573.

Chao, X., Shankar, N.J., Wang, Sam S.Y., 2003. Development and application of oil spill model for Singapore coastal waters. J. Hydraul. Eng. 129, 495–503.

Coppini, G., De Dominicis, M., Zodiatis, G., Lardner, R., Pinardi, N., Santoleri, R., Colella, S., Bignami, F., Hayes, D.R., Soloviev, D., Georgiou, G., Kallos, G., 2011. Hindcast of oil-spill pollution during the Lebanon crisis in the Eastern Mediterranean, July–August 2006. Mar. Pollut. Bull. 62 (1), 140–153.

Cucco, A., Sinerchia, M., Ribotti, A., Olita, A., Fazioli, L., Perilli, A., Sorgente, B., Borghini, M., Schroeder, K., Sorgente, R., 2012. A high-resolution real-time forecasting system for predicting the fate of oil spills in the Strait of Bonifacio (western Mediterranean Sea). Mar. Pollut. Bull. 64 (6), 1186–1200.

Delvigne, G.A.L., Sweeny, C.E., 1988. Natural dispersion of oil. Oil Chem. Pollut. 4, 281–310.

Gibbs, M.S., Dandy, G.C., Maier, H.R., 2008. A genetic algorithm calibration method based on convergence due to genetic drift. Inf. Sci. 178 (14), 2857–2869.

Gobeyn, S., Volk, M., Dominguez-Granda, L., Goethals, P.L., 2017. Input variable selection with a simple genetic algorithm for conceptual species distribution models: a case study of river pollution in Ecuador. Environ. Model. Softw. 92, 269–316.

Guo, W.J., Wang, Y.X., 2009. A numerical oil spill model based on a hybrid method. Mar. Pollut. Bull. 58, 726–734.

Guo, W.J., Wang, Y.X., Xie, M.X., Cui, Y.J., 2009. Modeling oil spill trajectory in coastal waters based on fractional Brownian motion. Mar. Pollut. Bull. 58 (9), 1339–1346.

Guo, W., Hao, Y., Zhang, L., Xu, T., Ren, X., Cao, F., Wang, S., 2014. Development and application of an oil spill model with wave–current interactions in coastal areas. Mar. Pollut. Bull. 84 (1), 213–224.

Guo, W., Wu, G., Liang, B., Xu, T., Chen, X., Yang, Z., Xie, M., Jiang, M., 2016. The influence of surface wave on water exchange in the Bohai Sea. Cont. Shelf Res. 118, 128–142.

Haupt, R.L., Haupt, S.E., 2004. Practical Genetic Algorithms, 2nd Edition. John Wiley & Sons.

Hodges, B., Orfila, A., Sayol, J., Hou, X., 2015. Operational oil spillmodeling: from science to engineering applications in the presence of uncertainty. In: Ehrhardt, M. (Ed.), Mathematical Modelling and Numerical Simulation of Oil Pollution Problems. The Reacting Atmosphere. vol. 2 Springer-Verlag.

Humphrey, B., Owens, E., Sergy, G., 1993. Development of a Stranded Oil in Coarse Sediment Model. Proceedings of the Oil Spill Conference, Washington, DC, pp. 573–582.

Huntley, H.S., Lipphardt Jr., B.L., Kirwan Jr., A.D., 2011. Surface drift predictions of the Deepwater Horizon spill: the Lagrangian perspective. In: Liu, Y. (Ed.), Monitoring and Modeling the Deepwater Horizon Oil Spill: A Record-breaking Enterprise. Geophys. Monogr. Ser., vol. 195. AGU, Washington, D.C., pp. 179–195. https://doi.org/10.1029/2011GM001097.

Korotenko, K.A., Mamedov, R.M., Kontar, A.E., Korotenko, L.A., 2004. Particle tracking method in the approach for prediction of oil slick transport in the sea: modelling oil pollution resulting from river input. J. Mar. Syst. 48 (1), 159–170.

Le Hénaff, M., Kourafalou, V.H., Paris, C.B., Helgers, J., Aman, Z.M., Hogan, P.J., Srinivasan, A., 2012. Surface evolution of the Deepwater horizon oil spill patch: combined effects of circulation and wind-induced drift. Environ. Sci. Technol. 46 (13), 7267–7273.

Lonin, S.A., 1999. Lagrangian model for oil spill diffusion at sea. Spill Sci. Technol. Bull. 5, 331–336.

Mackay, D., Paterson, S., Trudel, K., 1980. A Mathematical Model of Oil Spill Behaviour. Environment Canada, Environmental Protection Service, Environmental Impact Control Directorate, Environmental Emergency Branch, Research and Development Division.

Matsuzaki, Y., Fujita, I., 2017. In situ estimates of horizontal turbulent diffusivity at the sea surface for oil transport simulation. Mar. Pollut. Bull. 117 (1), 34–40.

Murray, S.P., 1972. Turbulent diffusion of oil in the ocean. Limnol. Oceanogr. 27, 651–660.

Nicklow, J.W., Reed, P.M., Savic, D., Dessalegne, T., Harrell, L., Chan-Hilton, A., Karamouz, M., Minsker, B., Ostfeld, A., Singh, A., Zechman, E., 2010. State of the art for genetic algorithms and beyond in water resources planning and management. J. Water Resour. Plan. Manag. 136 (4), 412–432.

Okubo, A., 1971. Oceanic diffusion diagrams. Deep-Sea Res. 18 (8), 789–802.

Phillips, O.M., 1977. Dynamics of the Upper Ocean, 2nd Edition. Cambridge University Press, pp. 336.

Proctor, R., Flather, R.A., Elliott, A.J., 1994. Modelling tides and surface drift in the Arabian Gulf—application to the Gulf oil spill. Cont. Shelf Res. 14 (5), 531–545.

Reed, M., 1989. The physical fates component of the natural resource damage assessment model system. Oil Chem. Pollut. 5 (2–3), 99–123.

Reed, M., Johansen, Ø., Brandvik, P.J., Daling, P., Lewis, A., Fiocco, R., Mackay, D., Prentki, R., 1999. Oil spill modeling towards the close of the 20th century: overview

of the state of the art. Spill Sci. Technol. Bull. 5 (1), 3–16.
Samuels, W.B., Huang, N.E., Amstutz, D.E., 1982. An oilspill trajectory analysis model with a variable wind deflection angle. Ocean Eng. 9, 347–360.
Shen, H.T., Yapa, P.D., 1988. Oil slick transport in rivers. J. Hydraul. Eng. 114 (5), 529–543.
Spaulding, M.L., 2017. State of the art review and future directions in oil spill modeling. Mar. Pollut. Bull. 115, 7–19.
Tkalich, P., Chan, E.S., 2002. Vertical mixing of oil droplets by breaking waves. Mar. Pollut. Bull. 44, 1219–1229.
Xu, H.L., Chen, J.N., Wang, S.D., Liu, Y., 2012. Oil spill forecast model based on uncertainty analysis: a case study of Dalian oil spill. Ocean Eng. 54, 206–212.
Yapa, P.D., 2005. Discussion of "Development and Application of Oil Spill Model for Singapore Coastal Waters" by Xiaobo Chao, N. Jothi Shankar, and Sam S. Y. Wang. J. Hydraul. Eng. 131 (1), 69–71.
Zhang, Y., Baptista, A.M., 2008. SELFE: a semi-implicit Eulerian–Lagrangian finite-element model for cross-scale ocean circulation. Ocean Model 21 (3), 71–96.